Journal of the Taiwan Institute of Chemical Engineers 118 (2021) 245–253

Contents lists available at ScienceDirect

Journal of the Taiwan Institute of Chemical Engineers

journal homepage: www.elsevier.com/locate/jtice

Cellulose acetate-MoS_2 nanopetal hybrid: A highly sensitive and selective electrochemical aptasensor of Troponin I for the early diagnosis of Acute Myocardial Infarction

Mugashini Vasudevan[a,b,*], Melvin J.Y. Tai[a,b], Veeradasan Perumal[a,b,*], Subash C.B. Gopinath[c], Satisvar Sundera Murthe[a,d], Mark Ovinis[b], Norani Muti Mohamed[a,d], Nirav Joshi[e,f]

[a] Centre of Innovative Nanostructures and Nanodevices (COINN), Universiti Teknologi PETRONAS, 32610 Seri Iskandar, Perak Darul Ridzuan, Malaysia
[b] Department of Mechanical Engineering, Universiti Teknologi PETRONAS, 32610 Seri Iskandar, Perak Darul Ridzuan, Malaysia
[c] Institute of Nano Electronic Engineering, Kangar 01000 & School of Bioprocess Engineering, Arau 02600, Universiti Malaysia Perlis (UniMAP), Perlis, Malaysia
[d] Department of Fundamental and Applied Sciences, Universiti Teknologi PETRONAS, 32610 Seri Iskandar, Perak Darul Ridzuan, Malaysia
[e] Sao Carlos Institute of Physics, University of Sao Paulo, CP 369, Sao Carlos 13560-970, Sao Paulo, Brazil
[f] Department of Mechanical Engineering, University of California, Berkeley, United States

ARTICLE INFO

Article History:
Received 26 September 2020
Revised 2 January 2021
Accepted 13 January 2021
Available online 19 January 2021

Keywords:
Electrochemical aptasensor
Cellulose acetate-molybdenum disulfide hybrid
Acute myocardial infarction
Troponin I

ABSTRACT

In this work, a novel aptamer-based CA-MoS_2 hybrid biosensor was developed for diagnosis of Acute Myocardial Infraction (AMI). Specifically, a novel petal-like MoS_2 nanoflower was used as the active material on the Screen-Printed Electrode (SPE) for AMI biomarker determination. The aptamer-based CA-MoS_2–24 hybrid was able to attain a low limit of detection (LOD) and sensitivity to 10 fM at a linear range from 10 fM to 1 nM with good reproducibility based on an electrochemical impedance spectroscopy and a ~4 folds higher selectivity of troponin I compared to the signal from other biomolecules in human serum, retaining a 91% stability after 6 weeks. This novel CA-MoS2 aptamer-based biosensor with a 2.3% RSD value has the potential to revolutionize medical diagnosis by conducting multiple biomolecule detection on a single sensing platform.

1. Introduction

Acute myocardial infarction (AMI) is a life-threatening cardiac disease when oxygenated blood flow to the heart is disrupted causing permanent injury to the heart tissues [1]. For good prognosis, early treatment is critical. Current clinical methods for the diagnosis of an AMI such as electrocardiogram (ECG), blood test, angiogram and echocardiogram are time consuming, have poor precision, are expensive and require sophisticated instrumentations [2]. Alternatively, a troponin I level of more than 0.1 ng mL^{-1} [3], a biomarker that is released in the blood stream from these damaged tissues after a heart attack, can be used to diagnose AMI. . While elevated levels of other biomarkers such as myoglobin, creatine-kinase MB, C-reactive protein, troponin T and troponin C are present in the blood stream after an AMI [1,4], troponin I is the standard and preferred biomarker for AMI diagnosis [3].

AMI biomarkers may be identified using electrochemical and optical methods such as surface plasmon resonance, chemiluminescence, aptasensor, fluorescence, colorimetric, enzyme-linked immunosorbent assay and immunosensors [5–7]. Electrochemical biosensing is considered a good method to diagnose AMI, as it has a wider measuring range, higher sensitivity and selectivity, simpler operation, faster response and lower cost compared to the optical methods.

Zuo et al. developed an electrochemical biosensor based on moleculary imprinted polymer (MIP) for the detection of troponin I, with a detection limit of 0.027 nM [8]. Jo et al. reported on troponin I detection via amperometry with a detection limit up to 1 pM, using sandwich aptamers and screen-printed carbon electrodes [9]. Aptamers are artificial nucleic acid ligands that are mostly used in clinical-based biosensors [10]. Aptamer-based biosensors are simple in construction, have high binding efficiency and provides a good response [11]. In another study, an AlGaN/GaN-based high electron mobility transistor (HEMT) biosensor developed by Sarangadharan et al. was used to detect highly sensitive cardiac troponin I [12] with a detection limit of 250 fM. On the other hand, Qiao et al. reported an electrochemical sensing platform based on aptamer-MoS_2 nanoconjugate with a 0.95 pM detection limit [13].

Molybdenum disulfide (MoS_2) is a promising transition metal dichalcogenide that has graphene-like morphology, with extensive applications in nanoelectronics, energy storage devices, super-

* Corresponding authors.
E-mail addresses: mugashini_18003585@utp.edu.my (M. Vasudevan), veeradasan.perumal@utp.edu.my (V. Perumal).

https://doi.org/10.1016/j.jtice.2021.01.016
1876-1070/

capacitors and biosensors. MoS_2 has a unique graphene-like sandwich structure of S-Mo-S, with triple layers held by van der Waals interactions [14,15], with the Mo and S molecules bound via covalent bonding. Transition metal sulphides are abundant, have large surface area, are biocompatible and are a cheap analogue to graphene [16,17]. It is a layered semiconductor (band hole = 1.2 eV, indirect) that withstands oxidation even in moist air at temperatures of up to 85°C [18] and poor cytotoxicity [19]. Furthermore, the layer spacing of MoS_2 (0.62 nm) , enhancing the sensitivity of a device tremendously when compared to the layer spacing of graphene (0.335 nm) [20]. These unique features make MoS_2 an important building block for biomarkers. Significant attempts have been made to develop MoS_2 nanomaterials with various morphological structures such as nanoparticles, nanoflower, nanosheets, nanoball, nanofibers and nanoflakes to enhance its sensitivity and selectivity.

MoS_2 is usually fabricated via a hydrothermal method and widely used as an active material in biosensors [21]. However, MoS_2 experiences severe restacking due to unstable van der Waals interaction, which significantly reduces its active sites and causes poor conductivity when combined with other conductive materials [22,23]. This leads to the poor energy density, which affects its functionality in the electrochemical biosensor [24]. To overcome these drawbacks, composite material bonding with MoS_2 is necessary. In a study, R.Rubio-Govea recently reported a laccase enzyme immobilised on flower-like and ribbon-like MoS_2 morphologies to determine the sensitivity and detection limit of dopamine in urine samples. The biosensor has a higher sensitivity of 340.3 nA/μM and a detection limit of up to 10 nM for the lacasse based ribbon-like MoS_2 biosensor compared to the flower-like MoS_2 [25]. M. Sadeghi showed that the coupling of MoS_2 nanosheets and PANI polymer enhances reproducibility and stability of an electrochemical biosensor [26]. Similarly, S. Kubendhiran demonstrated that the coupling of high conductivity PPy polymer and high catalytic activity of MoS_2 improves electrochemical performance because PPy polymer enhances the transport of electron property of the SPCEs modified electrode and further enhances the detection limit of berberine in rat plasma down to 5 μM [27]. Polymer nanofibers have excellent porosity and explicit space region [28,29], useful properties for a biosensor. A. Sinha et al. [30] found that the rapid electron transfer kinetics towards electrocatalysis of diverse targets occurs due to the strong anisotropy and edge plane active sites of MoS_2. Surface functionalization at edge plane active sites MoS_2 however, is required to improve their catalytic activity towards various redox processes.

The addition of carbon filled natural polymers in MoS_2 results in a hybrid microstructure capable of improving the electron transfer efficiency and thereby enhancing its conductivity properties [24,31]. In addition, to enhance the electrochemical performance of MoS_2, a natural carbon filled cellulose acetate (CA) nanofiber, fabricated by electrospinning technique, was coupled with MoS_2. CA has outstanding thermal stability, chemical resistance, biocompatibility, biodegradability and high interconnectivity [32,33]. However, CA is a poor conductive polymer, and hybridization of CA and MoS_2 could improve ita conductivity properties. Polymer intercalation between CA and MoS_2 can be achieved by linking CA filled with carbonyl and hydroxyl functional groups in MoS_2 [24]. These functional groups enable the attachment of MoS_2 precursor on the surface of CA nanofiber. The interaction of the functional groups and MoS_2 creates a new stable biosensing substrate for analytical detection.

CA bead-free nanofibers have been synthesized using a facile electrospinning. Subsequently, a CA-MoS_2 hybrid microstructure was synthesized via a low-cost hydrothermal method with a Mo precursor in conjugation with CA nanofibers at various treatment times (8, 16, and 24 h). MoS_2 was chosen because it has graphene-like chemical structure with excellent physical and chemical properties, rich surface chemistry, large surface area, is biocompatible and is a semiconductor material. On the other hand, CA has high mechanical strength, a large surface area, high binding affinity with other substances, is biodegradable, biocompatible, as well as displays excellent thermal and chemical stabilities. As such, a CA-MoS_2 hybrid was fabricated to enhance the electrical conductivity of CA and to overcome the drawbacks of MoS_2. MoS_2 petal-like nanosheets grew vertically on the surface of CA nanofibers due to the bonding of MoS_2 with the functional groups present in CA. This hybrid microstructure shows excellent electrical conductivity and numerous expose active sites, with good electron transfer and excellent electrochemical performance. The developed electrochemical aptamer-based CA-MoS_2 hybrid biosensor was able to detect Troponin I with high sensitivity, high selectivity and a low detection limit through the impedance spectroscopy analysis.

2. Materials and methods

2.1. Materials and reagents

The initial materials used were Cellulose Acetate (CA, MW = ~30,000 g mol^{-1}), 16 - Mercaptohexadecanoic acid, 1-Ethyl-3-(3-dimethylaminopropyl) carbodiimide (EDC), Silver Nanoparticles (AgNP), N-hydroxysuccinimide (NHS), Streptavidin, 1x Phosphate Buffered Saline (PBS) and (3-Aminopropyl) triethoxysilane (APTES), all obtained from Sigma-Aldrich Co., Ltd. (USA). Ammonium Heptamolybdate Tetrahydrate, Thiourea, Ethanolamine, Ethanol Absolute, Acetone and N,N-Dimethylformamide (DMF) were obtained from Merck & Co (USA). All the chemicals were used as received, without any purification steps. The Screen –Printed Electrode (SPE) transducer used in this study was commercially sourced and was purchased from Metrohm (Malaysia) Sdn. Bhd. The oligonucleotides were purchased from Avantis Laboratory (USA). The details of the oligonucleotide sequences utilized in this current work were as follows:

Probe (Aptamer) – 5′ – CGT GCA GTA CGC CAA CCT TTC TCA TGC GCT GCC CCT CTT AAA AAA AAA AAA AAA AAA AAA AAA A-3′; Biotin oligo linker – 5′ - / 5Biosg // iC6Sp / TTT TTT TTT TTT TTT TTT TT –3′ ; Target – Troponin I; Control – Troponin T; Human Serum of male AB plasma was purchased from Sigma-Aldrich Co., Ltd. (USA).

2.2. Synthesis of cellulose acetate (CA) solution

CA solution for electrospinning was prepared similar to that by Lee et al. [34]. Initially, 20 ml of DMF and 30 ml of acetone were measured through a measuring cylinder and poured into a 100 ml beaker. The solvent mixture was placed on a hot plate (DAIHAN Scientific, MSH-30D) and a magnetic bar was used to stir the solvent mixture for 10 min. 10.1 g of CA powder was gradually added in the stirred solvent mixture to prevent agglomeration. The mixture was continuously stirred for 12 h at room temperature to completely dissolve the cellulose acetate powder until a transparent polymer solution was produced.

2.3. Cellulose acetate (CA) nanofiber fabrication through electrospinning

The prepared CA solution was carefully injected into a 15 ml plastic syringe to prevent the formation of bubbles in the syringe. The parameters utilized in the electrospinning method are: 10 kV applied voltage, 15 cm tip to collector distance, and 0.4 ml h^{-1} flow rate. The electrospinning method was performed continuously for 12 h at room temperature to obtain a uniform nano size fibre thickness. The CA nanofibers was collected on an aluminium foil, and placed on a rotating collecting drum for ease of removal, and dried at 80 ° C.

2.4. CA-MoS_2 hybrid fabrication by hydrothermal method

A CA-MoS_2 hybrid was prepared using the hydrothermal method. To form CA-MoS_2, 0.1 g of CA nanofiber, 0.6 g of ammonium

heptamolybdate tetrahydrate and 1.77 g of thiourea were dissolved in 60 ml of distilled water and sonified for 30 min until a homogenous was obtained. The homogenous solution was then transferred into a 250 ml Teflon-lined stainless-steel autoclave and heated at a temperature of 200 ° C for 8, 16 and 24 h, respectively. After heating, the autoclave was left to cool for few hours. The resulting product, a black-coloured CA-MoS_2 hybrid, was collected via centrifugation using distilled water and ethanol absolute in sequence, for three times. The CA-MoS_2 hybrid precipitate was then dried in an oven at 60 °C for 12 h. The CA-MoS_2 hybrid sample was classified as CA-MoS_2-8, CA-MoS_2-16 and CA-MoS_2-24 based on the hydrothermal treatment time.

2.5. Surface modification on screen printed electrode (SPE)

The detection of Troponin I by aptamer using SPE electrode was conducted as follows: (i) 10 μL of 2% APTES was initially dropped on the bare SPE electrode to modify the SPE sensing surface area with amine surface and left for an hour; (ii) The amine sensing surface was further modified with a complex mixture containing 16-mercaptohexadecanoic acid, silver nanoparticle, NHS and EDC; (iii) 1 mg of functionalized CA-MoS_2 hybrid powder was dispersed in 1 mg of distilled water and dropped on CM/APTES/SPE modified electrode and left for 30 min; (iv) Streptavidin was carefully dropped on CA-MoS_2−24/CM/APTES/SPE modified surface and left for 30 min; (v) Ethanolamine (1 M) was coated on the Streptavidin/CA-MoS_2−24/CM/APTES/SPE for 30 min to block the non-specific site before immobilisation of the aptamer. A buffer solution 10 mM PBS of pH 7.4 was used to wash thoroughly after each modification. NHS and EDC were used to enhance and activate the modified SPE electrode. Impedance analysis was conducted to determine the chemical reaction of the assembled molecular on the surface modified electrode.

2.6. Immobilisation and interaction of troponin I

The CA-MoS_2-24 hybrid modified electrode was used to fabricate a protein biosensor to detect acute myocardial infarction (AMI). The direct immobilisation of aptamer onto CA-MoS_2−24 hybrid modified electrode was achieved by dropping 10 μL of biotin attached aptamer for 15 min, followed by washing the electrode with 10 mM PBS at pH 7.4. The troponin I interaction was successfully accomplished by dropping different concentrations (1 nM to 10 fM) of Troponin I on the aptamer modified CA-MoS_2-24 hybrid electrode. The unbound target was washed by buffer solution immediately after the interaction to avoid errors during measurements. Fig. 1 illustrates the complete immobilisation of biotin attached aptamer and its interaction with Troponin I. The hybridized electrode was stored at 4 °C when not in use [35]. The detail description on the dilution of biotinylated-oligo linker and aptamer is shown in the supplementary information.

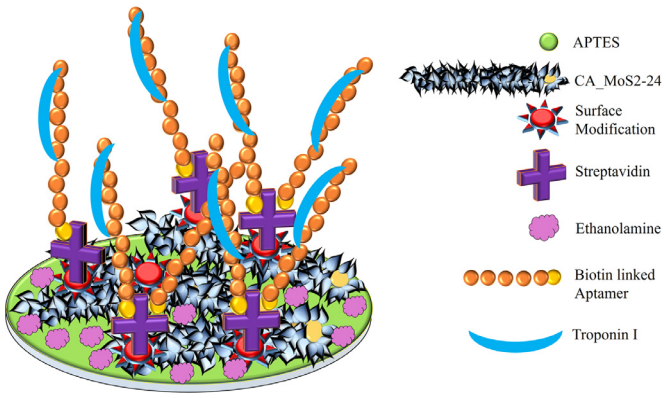

Fig. 1. Schematic illustration of the steps involved in the synthesis of the aptamer-based CA-MoS_2-24 hybrid microstructure on screen printed electrode (SPE).

2.7. Detection of troponin I in human serum

Human serum was diluted from 1:10 to 1:10,000 using 10 mM PBS at pH 7.4. These different dilutions of human serum were analysed through voltammetry to determine the ability of the aptamer modified CA-MoS_2-24 hybrid electrode to capture the specific target in human serum consisting of bundles of various biomolecules (Supplementary information Figure S1). A 1:10,000 dilution factor was chosen and used as a buffer solution to dilute the target at different concentrations (1 fM to 100 nM) to form Troponin I spiked sample, similar to section 2.6. The rest of the surface chemical modifications and detections strategies employed were identical to the previous methods.

2.8. Repeatability and stability analysis

The repeatability of the electrode was analysed by taking measurements using different electrodes to ensure that every electrode has approximately similar readings when the human serum was dropped on the aptamer modified CA-MoS_2−24 hybrid electrode. The stability of the interacted electrode was analysed on the weekly basis by dropping 10 μL of buffer solution on the surface of the electrode [36].

3. Results and discussion

3.1. Field-emission scanning electron microscopy (FESEM)

The surface morphology of the fabricated CA-MoS_2 hybrid nanofibers was characterized via FESEM. The CA-MoS_2 hybrid, synthesized by a hydrothermal method at different durations, were classified as CA-MoS_2-8, CA-MoS_2-16 and CA-MoS_2-24 respectively. The attachment of petal-like MoS_2 was attributed to the high surface roughness of the hybrid sample. Fig. 2 shows that the uniform petal-like MoS_2 nanosheets grew vertically, anchoring around the surface of the fabricated CA nanofiber for all three treatment times. The CA-MoS_2-8 hybrid nanofiber is 1.25 μm in diameter (Fig. 2a). The shape and size of MoS_2 nanoflower formed around the CA-MoS_2-8 hybrid nanofiber is not uniform and loosely arranged on the CA-MoS_2-8 hybrid nanofiber surface (Fig. 2b). The CA-MoS_2-16 hybrid, shown in Fig. 2c, has a larger diameter of 1.75 μm, due to more MoS_2 layers on the surface of the CA-MoS_2-16 hybrid. There is two long loosely arranged CA-MoS_2-16 hybrid nanofibers, resulting in an uneven shape and irregular size of the MoS_2 nanoflower (Fig. 2d). MoS_2 is abundant in the CA-MoS_2-24 hybrid nanofibers, as shown in Fig. 2e. The heterogeneous growth of the MoS_2 petal-like nanosheets perpendicular to the surface of CA nanofiber results in a larger diameter, dense MoS_2 petal-like nanosheets with significant active site edge exposure compared to the hybrid nanoflowers for other treatment time [37]. The 2.25 μm diameter of CA-MoS_2-24 is a significant increase in surface area. Moreover, MoS_2 petal like nanosheets are well stacked, due to van der Waals interaction, which induces the formation of MoS_2 nanoflower on the surface of the CA-MoS_2 hybrid nanofibers (Fig. 2f) [23]. The TEM characterization is provided in the supplementary information (Figure S2). The amount of flower-like structures of MoS_2 attached on the surface of the hybrid nanofiber increases with increasing hydrothermal treatment time (Fig. 2). Fig. 2f shows the closely arranged hybrid nanofiber consisting of many specific active areas, especially when the one-dimensional (1D) cellulose acetate nanofiber and 2D MoS_2 flower-like nanosheets forms a 3D microstructure, which provides for a large number of probes during the immobilisation and interaction processes [38]. These FESEM images prove that as hydrothermal treatment time increases, the diameter of

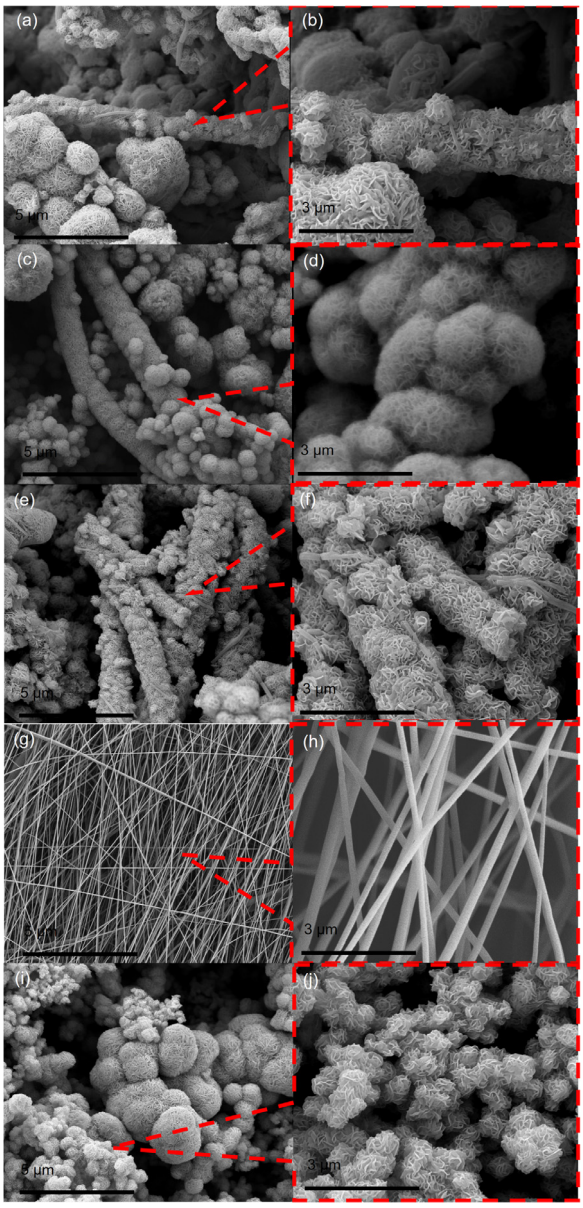

Fig. 2. FESEM images of CA-MoS_2 hybrid microstructure. (a) Low and (b) high magnifications images at 8 h treatment; (c) Low and (d) high magnifications at 16 h treatment and (e) Low and (f) high magnifications at 24 h treatment. FESEM images of (g) Low and (h) high magnifications of CA. FESEM image of (i) Low and (j) high magnifications of bare MoS_2 nanoflower were shown. The scanning electron microscope uses a focused beam of high-energy electrons up to 30 kV.

the hybrid CA-MoS_2 increases. The morphology of the CA nanofiber obtained through the electrospinning technique was determined before proceeding to the hydrothermal method (Fig. 2g). The CA nanofibers exhibit a uniform structure, with a high surface area. These uniform and bead-free nanofibers have the smallest diameters, ranging from 100 nm to 200 nm (Fig. 2h). The bare MoS_2 shown in Fig. 2i has an irregular flower-like shape and size. The high magnification image in Fig. 2j show that the MoS_2 is aggregated due to van der Waals interaction forming a 3D flower-like structure. The structure has many effective sites due to its wider and uneven structure, which facilitates the interaction of probe and bio-target in detecting Troponin I.

3.1.1. X-ray diffraction (XRD)

The crystallinity and plane orientation of the synthesized CA-MoS_2 hybrid at different hydrothermal treatment times were analysed via XRD. As shown in Fig. 3(a-e), the diffraction peaks obtained

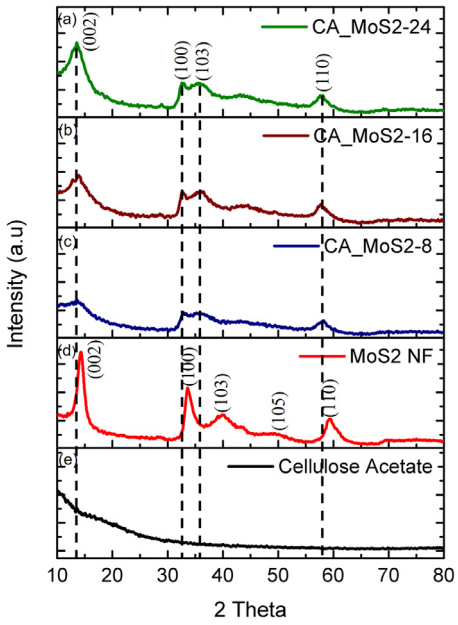

Fig. 3. XRD images of (a) CA-MoS_2 hybrid microstructure at 24 h treatment; (b) CA-MoS2 hybrid microstructure at 16 h treatment; (c) CA-MoS_2 hybrid microstructure at 8 h treatment; (d) MoS_2 NF and (e) CA. Showing the semi-crystalline peaks of fabricated microstructures.

for the CA-MoS_2 hybrids at 8, 16 and 24 h were compared with bare MoS_2 NF and CA. The peaks spotted for CA-MoS_2-8 (Fig. 3c), CA-MoS_2−16 (Fig. 3b) and CA-MoS_2-24 (Fig. 3a), are the hexagonal phase of MoS_2 (JCPDS 37-1492), with diffraction peaks at 12.0° (002), 33.1° (100), 37.2° (103) and 58.1° (110). The peak sharpness at (002) plane increases as the hydrothermal time increases, indicative of the crystallinity of the sample, with high intensity peaks corresponding to excellent crystallinity. The (002) plane corresponds to few single layers of MoS_2 and are also responsible for the principal characteristics of the semi-crystalline acetylated structure of CA [39–41]. The layers of MoS_2 in hybrid microstructure can be clearly observed using TEM analysis, as shown in supplementary information (Figure S2). The diffraction peaks of CA-MoS_2-8, CA-MoS_2-16 and CA-MoS_2-24 were slightly lower compared to the peaks for bare MoS_2 NF (Fig. 3d), due to CA coupling with bare MoS_2 NF. The expansion of d-spacing and the presence of strains contributes to variations in peaks [42]. There were no obvious peaks found for CA due to its amorphous nature.

3.2. Fourier-transform infrared spectroscopy (FT-IR)

Fig. 4 (a-e) shows the FT-IR analysis of CA (Fig. 4e), MoS_2 – NF (Fig. 4d) and CA-MoS_2 hybrids at 8 (Fig. 4c), 16 (Fig. 4b), and 24 h (Fig. 4a). The absorption peaks of CA-MoS_2 hybrid at different durations are 435.6, 667.4, 758.2, 901.6, 1103.4, 1398.2, 1603.3, 1728.36, 3118.5 and 3436 cm^{-1}. Assuming that the Mo-S stretching vibration mode is at peak 435.6 cm^1 and the asymmetric vibration of the Mo-O group peaks at 667.4 cm^1, bands 758.2 and 901.6 cm^{-1} reveal the existence of stretching and bending vibration of the S-S and C—H bond respectively. The absorption peak at 1103.4 cm^{-1} might be due to the Mo-O group and C—O bending, whereas the bands observed at 1398.2 cm^1 are due to O—H bending and $S = O$ stretching. At 1603.3 cm^{-1} and 1728.3 cm^{-1}, the absorption peaks represent the $C = C$ bond and aldehyde group respectively, which suggests the presence of CA in the hybrid heterostructure. The broad and prominent peaks at 3118.5 and 3426 cm^{-1} are the result of the stretching of the O—H bond. The FT-IR analysis of CA-MoS_2 hybrid has validated the successful

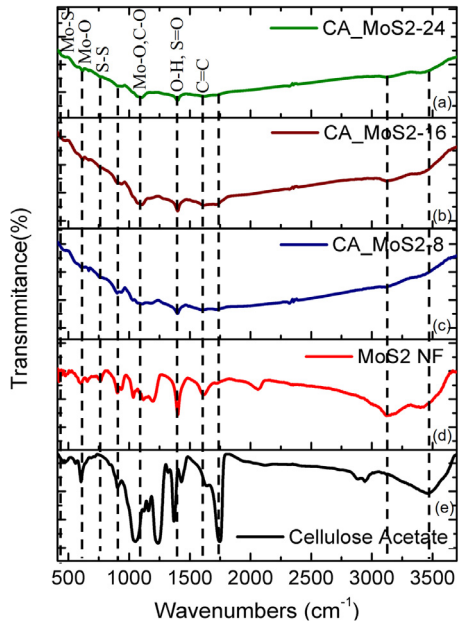

Fig. 4. FT-IR spectra images of fabricated (a) CA-MoS_2 hybrid microstructure at 24 h treatment; (b) CA-MoS_2 hybrid microstructure at 16 h treatment; (c) CA-MoS_2 hybrid microstructure at 8 h treatment;(d) MoS2 NF and (e) CA. Absorption regions are shown from 350 to 3700 cm-1.

pairing of MoS_2 NF and CA in the fabricated hybrid nanofiber via the hydrothermal method [43,44].

3.3. Surface modification on SPE electrode

The screen-printed electrode (SPE) was modified to enable immobilisation of probe. The resistance charge transfer (Rct) of the layer by layer modification was analysed via electrochemical impedance spectroscopy (EIS) and the resulting Nyquist plots are shown in Fig. 5a. At the low frequency region, the semicircle of the CA-MoS_2 in the impedance spectrum representing the Rct (0.017 MΩ) corresponds to the presence of a unique hybrid structure forming an intimate interface contact between the petal-like MoS_2 and the cellulose acetate nanofiber, which provides a diffusion path to enhance the charge transfer by improving the electrical conductivity of the hybrid. Moreover, the MoS_2 filled polymer has a high intrinsic conductivity that leads to high energy density, which improves the electron transport in the microstructure MoS_2 electrode. With increase surface modification (SM), the Rct value increases. These modifications enable CA-MoS_2 to bond with streptavidin via silver nanoparticles (Ag NPs), which acts as a linkage between materials. Furthermore, the Ag NPs increased the surface area, improving biomolecules interaction. The oxophilicity of the hybrid material can be ameliorated by adding Ag NPs, which boost the charge transfer between materials and the liquid based sensing performance [45]. This step enhances the performance of the sensor, which significantly improves sensitivity.

A good improvement in the Rct (0.052 MΩ) value was observed upon dropping streptavidin on the CA-MoS_2/SM modified SPE. The observed increment in charge transfer resistance indicates that streptavidin has successfully attached on the CA-MoS_2/SM modified SPE. Chemical interaction between streptavidin and CA-MoS_2 hybrid enables rapid electron transfer in the electrode.

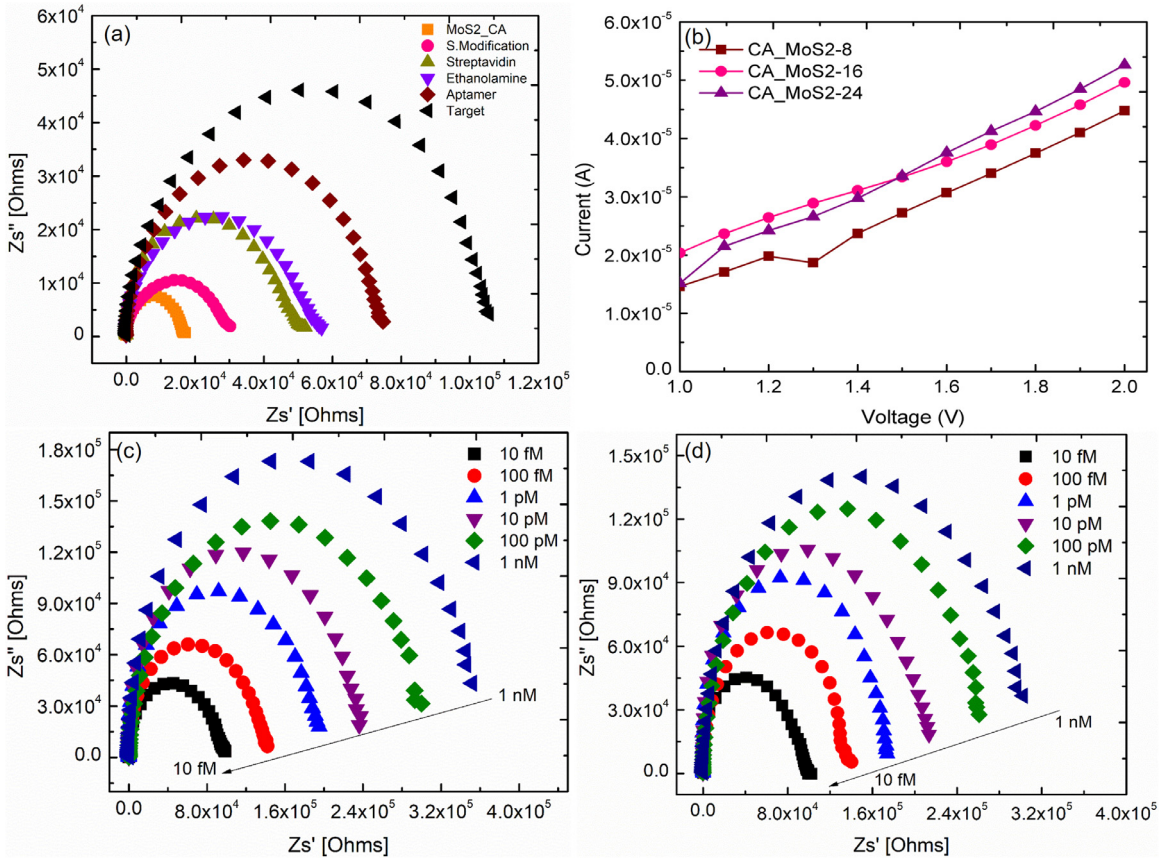

Fig. 5. (a) Nyquist plot on surface modifications on SPE electrode. (b) Voltammetry (I-V) reading of CA-MoS_2 hybrid nanofibers at 8 h, 16 h and 24 h electrodes in the voltage at 2 V. c) Analysis on limit of detection. Different concentrations of target (1 pM to 10 fM) through impedance spectroscopy analysis were shown. (d) Impedance spectra measurement. It is to identify the selectivity of the biosensor. Human serum in the presence of other biomolecules was tested.

When ethanolamine as a blocking agent was dropped, there was an insignificant increase in Rct (0.057 MΩ). This blocking agent is able to obstruct the unreacted structure, preventing bio-fouling. The biotin-aptamer has bounded strongly with the four binding sites of streptavidin, causing the streptavidin-aptamer complex formation to be high [46]. This complex formation was revealed when the Rct (0.075 MΩ) value of streptavidin increase significantly, indicative of successful immobilisation of the probe. An increase of 0.031 MΩ to the streptavidin Rct value shows that the interaction of Troponin I on aptamer modified electrode surface occurred and bio-sensing of the developed biosensor was established.

The Electrochemical Impedances Spectroscopy (EIS) measurement for surface modification on SPE to detect troponin I was carried out in a redox free environment with parameters plotted as Zimaginary vs Zreal. The Nyquist plot shown in Fig. 5a reveals the steps involved in each chemical modification on the developed sensor. The low frequency semicircle in the Nyquist plot correlate to the diffusion-limited processes, whereas the high frequency semicircle correlated to the finite electron transfer process [47]. The variation in the electrochemical signal during surface modification is due to disparity in the material–electrolyte interface properties and the electrolyte ion diffusion rates during the charge–discharge processes [48]. Continuous surface modification reduce the effective sensing surface of SPE. The semicircles in the Nyquist plot represent the charge transfer resistances (Rct) on the sensing surface as the number of modification layer increases. The addition of targets further induces the charge transfer resistance due to the electrostatic repulsion during the hybridization of the probe-target. The biosensor was modelled as an Randles equivalent circuit , which consists of charge transfer resistance (Rct), Constant Phase Elements (CPE), and Warburg impedance (W) [49]. The CPE indicates the double layer formation and is widely used for data fitting of electrochemical impedances, whereas the Warburg impedance represents the diffusion of redox between solid and liquid interface [50,51]. The equivalent circuit for the step-by-step surface modification in Fig. 5a is shown in Supplementary Information Table S2. The change in the Rct value corresponds to the transfer of electron and ions charges. The sinusoidal perturbation in EIS was 1 V rms.

The CA polymer fibres in the solution were surrounded by charged ions, whereby the positive ions are attracted to the functional group of fibre surface due to the π-electron interaction from the fibres and the negatively charged molybdenum compounds were attracted to the positively charged fibre surface, which causes sub-oxidation to occur and reduce the compounds to MoS and H_2S (thiourea) during the hydrothermal process [23]. Due to the formation of nucleation sites, the molybdenum compounds were attracted to the surface of fibres. The low surface energy (002) planes of MoS_2 resulted in few layers of MoS_2 growing on the surface of fibres. The strong coordination bond between the transition metal Mo with the functional group present in cellulose acetate facilitated the development of MoS_2 on the surface of the CA nanofiber. CA acts as a substrate for the formation petal-like structure on the surface of CA due to the electrostatic interaction between negatively charged basal plane MoS_2 and positively charged aromatic groups of CA [52].

3.4. Selection of CA-MoS_2 hybrid via voltammetry analysis

The conductivity and resistivity of the CA-MoS_2 hybrid was determined using voltammetry. Fig. 5b shows the current versus voltage readings of the CA-MoS_2 hybrid at 8, 16 and 24 h on APTES and modified SPE electrodes. At 2 V, the current measured for CA-MoS_2-8, CA-MoS_2-16 and CA-MoS_2-24 were 4.5 X 10^{-5} A, 5.0 X 10^{-5} A and 5.3 X 10^{-5} A respectively. With increasing hydrothermal time, the electrical conductivity of the hybrid materials increases. MoS_2 has a tuneable electronic energy states, which causes the accumulation of charges to occur. Higher current due to high conductivity rate with low resistivity results in a low gradient value for the CA-MoS_2-24 hybrid. As the electrical conductivity increases, the resistivity reduces, making the CA-MoS_2-24 hybrid the best hybrid material for immobilisation and hybridisation of probe and bio target to detect Troponin I.

3.5. Biomolecular interaction analyses by impedance spectroscopy

Troponin I interaction studies have been conducted by exposing aptamer-modified bio-electrode with various concentrations of Troponin I (1 nM to 10 fM), to determine the limit of detection, as shown in the Nyquist plot (Fig. 5c). The interaction of Troponin I on aptamer modified bio-electrode increases as the concentration increases, which reduces the charge transfer resistance, as the target concentration increases. At low frequency, the lowest target concentration of 10 fM registered an impedance, meaning that the protein-binding nucleotide sequences (Aptamer) have high affinity against Troponin I even at concentration levels as low as 10 fM, equivalent to 0.24 pg/mL. When Troponin I is present in the sensing surface, aptamer had a rigid and definite tertiary structure due to specific binding with target [13]. A summary of previous studies based on strategy and the method used to detect troponin I are shown in the supplementary information in Table S1.

3.6. Specificity and validation with human serum

The specificity of aptamer-modified bio-electrode was evaluated by dropping different concentrations of human serum on the sensing surface of the prepared bio-electrode under the same experimental conditions as the target. The Nyquist plot, as shown in Fig. 5d, shows a similar sequence trend as the target, where the Rct value increases upon interaction with increasing concentrations of the target in human serum. These results indicate that the biosensor exhibits a high specificity for Troponin I detection in human serum, although there is an abundance of other protein biomolecules in the human serum. The performance of the developed biosensor was compared with previously reported biosensors for Troponin I detection and displayed in the supplementary information in Table S1. The fabricated biosensor is more sensitive and selective compared to other biosensors.

3.7. Analytical performances of the CA-MoS_2 hybrid biosensor

The analytical performance of the aptamer-based CA-MoS_2 hybrid bio-electrode was further investigated and the results are shown in Fig. 6(a-d). The developed biosensor has a limit of detection up to 10fM, as shown in section 3.7 from the impedance analysis during the hybridization of Troponin I. Troponin I level in a normal healthy human is <0.04 ng/ml and >0.40 ng/ml after an AMI, well within the limit of detection for the current biosensor.

The linear regression, R^2 as shown in Fig. 6a, is 0.9976, which shows that the sensor has good linearity with target Troponin I and concentration increment. The sensitivity, which is given by:

$$Sensitivity = \frac{\text{Slope of calibration plot, m}\left(\mu\text{A mM}^{-1}\right)}{\text{Active Surface Area, A (cm}^2\text{)}}$$

is 39.34 μA mM^{-1} cm^{-2} for a SPE active surface area of 0.1257cm^2. The limit of detection and sensitivity of the developed hybrid biosensor is better compared to that of previous studies, as shown in supplementary information in Table S1. Furthermore, for selectivity with other biomolecules, the Rct value for interaction was ~5 folds higher than the Rct value for immobilisation, as shown in Fig. 6b. These results indicate that the designed nucleic acid probe binds only to the specific and selected protein, which shows that the Aptamer-Troponin I interaction is very selective. The difference in Rct value between the control (1 nM) and Troponin I in human serum (1 nM) is ~4 folds, with the aptamer detecting Troponin I even though there were other

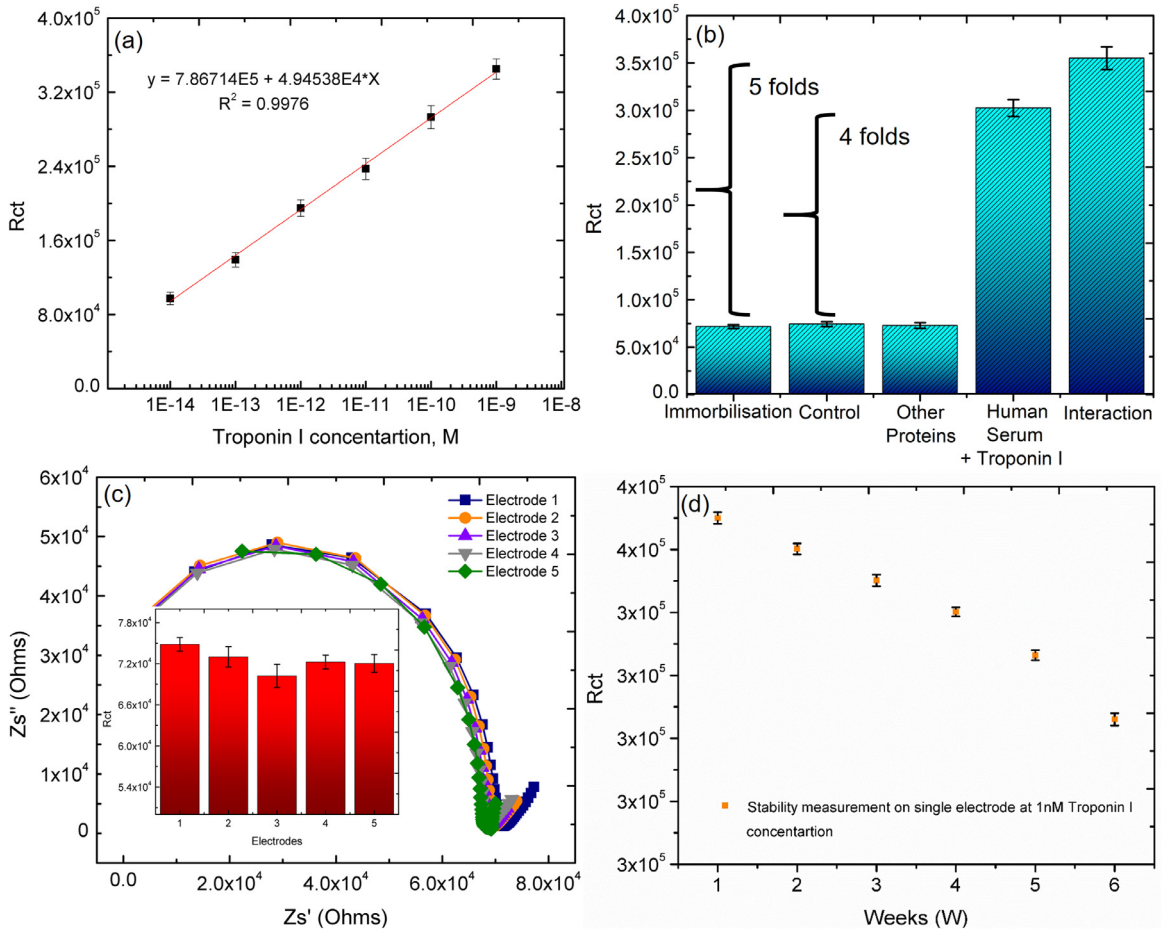

Fig. 6. (a) Linear regression curve. Different concentrations of target with a linear equation of ΔRct; (b) A bar diagram on selectivity of the biosensor and its Rct value; (c) Reproducibility of the biosensor using 5 different SPE electrodes. Inset graph is showing the bar chart of reproducibility of 5 electrodes. (d) Stability of the biosensor. Tested for 6 weeks against Rct was shown.

proteins (albumin, globulin, regulatory proteins) in the human serum together with Troponin I. There was no obvious change in Rct value for the control Troponin T (0.074 MΩ) and other proteins (0.073 MΩ), suggesting little or no interaction has taken place. The repeatability curve in Fig. 6c of aptamer-based CA-MoS_2 hybrid bio-electrode has a relative standard deviation (RSD) of 2.3%, with 5 electrodes prepared under the similar processing conditions. The bar chart shown in the insert shows that there is no significant differences between the 5 electrodes when parallel measurements were taken. The hybridized SPE electrode was stored at 4 °C when not in use to maintain the device capability and to avoid contamination. Fig. 6d depicts the stability of an electrode for 6 weeks. The developed biosensor shows high stability despite a 6-week time lapse and retains up to 91% of the impedance signal. After a period of 6 weeks, the biosensing device only loses 9% of its sensing capability.

3.8. Novelty and biosensing mechanism

Electrochemical aptasensing is a quick and simple method for detection of biological analyte. However, the efficacy of a biosensor depends greatly on the transducer, active materials, probe, and analyte. The novelty of the present work is the development of a highly sensitive and selective electrochemical aptasensor of troponin I based on a chemically modified cellulose acetate-MoS_2 nanopetal hybrid-biotin linked aptamer on SPE. The developed biosensor has 5 times higher selectivity at 39.34 μA mM^{-1} cm^{-2}, as shown in Fig. 6b, with the lowest limit of detection of 10fM equivalent to 0.24 pg/mL thus far, as shown in supplementary information Table S1. We have successfully grown MoS_2 nanoflower on smooth, un-beaded cellulose acetate nanofiber surface through a finely tuned hydrothermal method. CA nanofiber was assembled using optimum parameters via ultrafine fibre production method (electrospinning). Through FESEM observation, the hybrid nanofiber diameter was found to increase with increasing treatment periods (8, 16, 24 hrs). CA-MoS_2 hybrid fabrication was done for the first time and it brought benefits in enhancing the conductivity of cellulose acetate biopolymer and molybdenum disulfide composite to detect Troponin I. CA is a poor conductive polymer but has numerous functional groups with excellent thermal and chemical stabilities, as well as high binding affinity with other substances, which makes it a suitable polymer to form a hybrid material with MoS_2. On the other hand, MoS_2 is a semi-conducting material but experiences severe stacking and restacking limitations due to unstable van der Waals interaction, which significantly reduces its active sites and causes poor conductivity. Thus, the covalent coupling of CA-MoS_2 hybrid through a finely tuned hydrothermal process overcomes the drawbacks of MoS_2 and enhances the intrinsic electrical conductivity, without disrupting charge transport. Numerous functional groups in CA and the rich surface chemistry of MoS_2 causes MoS_2 to grow on CA, forming flower-like MoS_2 on CA nanofiber polymer. Furthermore, owing to the large semi-conductive non-stacking surface area-to-volume ratio of the CA-MoS_2 hybrid, more active sites were formed, which facilitates the surface modification and immobilization of Aptamers onto the CA-MoS2 hybrid, altering the dynamic equilibrium of the conductivity. This results in a decrease in electron concentration transfer, leading to a broadening of the depletion layer, which lowers the conductivity of each SPE

modified layer. Surface modification of the active sites of the CA-MoS2 hybrid electrode is necessary to improve its chemical reactivity during probe-target interaction. Hence, the electrochemical performance improves significantly with the CA-MoS_2 hybrid as MoS_2 induces the transfer of electron properties of the modified SPE, which further enhances electrical conductivity for Troponin I detection.

Conclusion

In summary, a novel CA-MoS_2 hybrid aptamer-based biosensor for the detection of Troponin 1 biomarker with a detection limit of up to 10 fM and a ~4 fold improvement in selectivity was developed via the hydrothermal method, using a bottom-up and top-down approach. The CA-MoS_2 hybrid has a large electroactive surface area and fast electron transfer, which improves electrochemical performance. The detection limit is 10 fM, with high stability of 91% for 6 weeks, when the electrodes are stored at 4 °C. The developed biosensor has excellent sensitivity and selectivity, as it is able to detect Troponin I at concentrations as low as 10 fM in human serum with other biomolecules present. The CA-MoS_2 hybrid can be developed further to detect multiple biological molecules and a wide range of clinical biomarkers for a point-of-care analysis. A new approach in improving the early diagnosis of AMI could improve prognosis. It is a promising alternative method for early AMI diagnosis. However, the limitation faced in this research was the usage of SPE as transducer Design and development of a bespoke electrode, which would be more sensitive, could potentially enhance bio-capturing efficiency.

Declaration of competing interest

None

Acknowledgments

Thanking note to Universiti Teknologi Petronas (UTP) for the financial support provided through URIF Grant (015LBO-021) and for giving chance to carry out the research in Nanotechnology Research Laboratory and Dye Solar Cell Laboratory. The authors also would like to thank Universiti Malaysia Perlis for providing the facilities and opportunity to conduct voltammetry experiment at Institute of Nano Electronic Engineering.

Author Contributions

Fabrication and development of hybrid microstructures were conducted by M.V. Experiments and drafted manuscript were carried out by M.V with the help of M.T, S.C.B.G, S.S.M, M.O, N.M.M and N.J proofread the manuscript. V.P supervised the work. All authors analysed the results and contributed to the discussion presented in the manuscript.

Additional Information

The authors declare no competing financial interests.

Supplementary materials

Supplementary material associated with this article can be found, in the online version, at doi:10.1016/j.jtice.2021.01.016.

References

[1] Regan B, O'Kennedy R, Collins D. Point-of-care compatibility of ultra-sensitive detection techniques for the cardiac biomarker troponin I—Challenges and potential value. Biosensors 2018;8:1–32. doi: 10.3390/bios8040114.
[2] Fathil MFM, Md Arshad MK, Gopinath SCB, Hashim U, Adzhri R, Ayub RM, Ruslinda AR, Nuzaihan M, Azman AH, Zaki M, Tang TH. Diagnostics on acute myocardial infarction: cardiac troponin biomarkers. Biosens Bioelectron 2015;70:209–20. doi: 10.1016/j.bios.2015.03.037.
[3] Hospital S. H. Biosciences, original 1. J Med Investig 2018;53:34–41.
[4] Jo H, Gu H, Jeon W, Youn H, Her J, Kim SK, Lee J, Shin JH, Ban C. Electrochemical aptasensor of cardiac troponin i for the early diagnosis of acute myocardial infarction. Anal Chem 2015;87:9869–75. doi: 10.1021/acs.analchem.5b02312.
[5] Tadepalli S, Kuang Z, Jiang Q, Liu KK, Fisher MA, Morrissey JJ, Kharasch ED, Slocik JM, Naik RR, Singamaneni S. Peptide functionalized gold nanorods for the sensitive detection of a cardiac biomarker using plasmonic paper devices. Sci Rep 2015;5:1–11. doi: 10.1038/srep16206.
[6] Perumal V, Hashim U. Advances in biosensors: principle, architecture and applications. J Appl Biomed 2014;12:1–15. doi: 10.1016/j.jab.2013.02.001.
[7] Ahmad K, Kumar P, Mobin SM. A highly sensitive and selective hydroquinone sensor based on a newly designed N-rGO/SrZrO3 composite. Nanoscale Adv 2020;2:502–11. doi: 10.1039/c9na00573k.
[8] Zuo J, Zhao X, Ju X, Qiu S, Hu W, Fan T, Zhang J. A new molecularly imprinted polymer (mip)-based electrochemical sensor for monitoring cardiac troponin I (cTnI) in the serum. Electroanalysis 2016;28:2044–9. doi: 10.1002/elan.201600059.
[9] Jo H, Her J, Lee H, Shim YB, Ban C. Highly sensitive amperometric detection of cardiac troponin I using sandwich aptamers and screen-printed carbon electrodes. Talanta 2017;165:442–8. doi: 10.1016/j.talanta.2016.12.091.
[10] Gopinath SCB, Lakshmipriya T, Chen Y, Phang WM, Hashim U. Aptamer-based "point-of-care testing. Biotechnol Adv 2016;34:198–208. doi: 10.1016/j.biotechadv.2016.02.003.
[11] Gopinath SCB, Lakshmipriya T, Awazu K. Colorimetric detection of controlled assembly and disassembly of aptamers on unmodified gold nanoparticles. Biosens Bioelectron 2014;51:115–23. doi: 10.1016/j.bios.2013.07.037.
[12] Sarangadharan I, Regmi A, Chen YW, Hsu CP, chi Chen P, Chang WH, Lee GY, Chyi JI, Shiesh SC, Bin Lee G, Wang YL. High sensitivity cardiac troponin I detection in physiological environment using AlGaN/GaN high electron mobility transistor (HEMT) biosensors. Biosens Bioelectron 2018;100:282–9. doi: 10.1016/j.bios.2017.09.018.
[13] Qiao X, Li K, Xu J, Cheng N, Sheng Q, Cao W, Yue T, Zheng J. Novel electrochemical sensing platform for ultrasensitive detection of cardiac troponin I based on aptamer-MoS2 nanoconjugates. Biosens Bioelectron 2018;113:142–7. doi: 10.1016/j.bios.2018.05.003.
[14] Lin X, Ni Y, Kokot S. Electrochemical and bio-sensing platform based on a novel 3D Cu nano-flowers/layered MoS2 composite. Biosens Bioelectron 2016;79:685–92. doi: 10.1016/j.bios.2015.12.072.
[15] Wang D, Pan Z, Wu Z, Wang Z, Liu Z. Hydrothermal synthesis of MoS_2 nanoflowers as highly efficient hydrogen evolution reaction catalysts. J. Power Sources. 2014;264:229–34. doi: 10.1016/j.jpowsour.2014.04.066.
[16] Parra-Alfambra AM, Casero E, Vázquez L, Quintana C, del Pozo M, Petit-Domínguez MD. MoS_2 nanosheets for improving analytical performance of lactate biosensors. Sens Actuat, B Chem 2018;274:310–7. doi: 10.1016/j.snb.2018.07.124.
[17] Anderson K, Poulter B, Dudgeon J, Li SE, Ma X. A highly sensitive nonenzymatic glucose biosensor based on the regulatory effect of glucose on electrochemical behaviors of colloidal silver nanoparticles on MoS_2. Sensors 2017(Switzerland):17. doi: 10.3390/s17081807.
[18] Goud BS, Koyyada G, Jung JH, Reddy GR, Shim J, Nam ND, Vattikuti SVP. Surface oxygen vacancy facilitated Z-scheme MoS2/Bi2O3 heterojunction for enhanced visible-light driven photocatalysis-pollutant degradation and hydrogen production. Int J Hydrog Energy 2020;45:18961–75. doi: 10.1016/j.ijhydene.2020.05.073.
[19] Zhu D, Huang J, Lu B, Zhu Y, Wei Y, Zhang Q, Guo X, Yuwen L, Su S, Chao J, Wang L. Intracellular micro RNA imaging with MoS_2-supported nonenzymatic catassembly of DNA hairpins. ACS Appl Mater Interfaces 2019;11:20725–33. doi: 10.1021/acsami.9b04883.
[20] Murugan N, Kumar THV, Devi NR, Sundramoorthy AK. A flower-structured MoS_2-decorated f-MWCNTs/ZnO hybrid nanocomposite-modified sensor for the selective electrochemical detection of vitamin C. New J Chem 2019;43:15105–14. doi: 10.1039/c9nj02993a.
[21] Su S, Sun Q, Wan L, Gu X, Zhu D, Zhou Y, Chao J, Wang L. Ultrasensitive analysis of carcinoembryonic antigen based on MoS2-based electrochemical immunosensor with triple signal amplification. Biosens Bioelectron 2019;140:2–7. doi: 10.1016/j.bios.2019.111353.
[22] Cao J, Zhou J, Zhang Y, Liu X. A clean and facile synthesis strategy of MoS_2 nanosheets grown on multi-wall CNTs for enhanced hydrogen evolution reaction performance. Sci Rep 2017;7:1–8. doi: 10.1038/s41598-017-09047-x.
[23] Sari FNI, Ting JM. Direct growth of MoS_2 nanowalls on carbon nanofibers for use in supercapacitor. Sci Rep 2017;7:1–13. doi: 10.1038/s41598-017-05805-z.
[24] Zeng X, Niu L, Song L, Wang X, Shi X, Yan J. Effect of polymer addition on the structure and hydrogen evolution reaction property of nanoflower-like molybdenum disulfide. Metals (Basel) 2015;5:1829–44. doi: 10.3390/met5041829.
[25] Rubio-Govea R, Hickey DP, García-Morales R, Rodriguez-Delgado M, Domínguez-Rovira MA, Minteer SD, Ornelas-Soto N, García-García A. MoS2 nanostructured materials for electrode modification in the development of a laccase based amperometric biosensor for non-invasive dopamine detection. Microchem J 2020;155:104792. doi: 10.1016/j.microc.2020.104792.
[26] Sadeghi M, Jahanshahi M, Javadian H. Highly sensitive biosensor for detection of DNA nucleobases: enhanced electrochemical sensing based on polyaniline/single-layer MoS2 nanosheets nanocomposite modified carbon paste electrode. Microchem J 2020;152:104315. doi: 10.1016/j.microc.2019.104315.
[27] Kubendhiran S, Lai J, Tsai H, Chen M. Electroactive polypyrrole-molybdenum disulfide nanocomposite for ultrasensitive detection of berberine in rat plasma. Anal. Chim. Acta. 2020. doi: 10.1016/j.aca.2020.05.056.

[28] Son WK, Youk JH, Park WH. Antimicrobial cellulose acetate nanofibers containing silver nanoparticles. Carbohydr Polym 2006;65:430–4. doi: 10.1016/j.carbpol.2006.01.037.
[29] Wang F, Liu H, Hu K, Li Y, Zeng W, Zeng L. Hierarchical composites of MoS2 nanoflower anchored on SnO_2 nanofiber for methane sensing. Ceram Int 2019;45:22981–6. doi: 10.1016/j.ceramint.2019.07.342.
[30] Sinha A, Dhanjai BTan, Huang Y, Zhao H, Dang X, Chen J, Jain R. MoS_2 nanostructures for electrochemical sensing of multidisciplinary targets: a review. TrAC - Trends Anal Chem 2018;102:75–90. doi: 10.1016/j.trac.2018.01.008.
[31] Qianwen M, Yaping D, Li L, Anqing W, Dingding D, Yijun Z. Electrospun MoS_2 composite carbon nanofibers for determination of vanillin. J Electroanal Chem 2019;833:297–303. doi: 10.1016/j.jelechem.2018.09.040.
[32] Aboamera NM, Mohamed A, Salama A, Khattab A. Characterization and mechanical properties of electrospun cellulose acetate/graphene oxide composite nanofibers. Mech Adv Mater Struct 2019;26:765–9. doi: 10.1080/15376494.2017.1410914.
[33] Khan SB, Alamry KA, Bifari EN, Asiri AM, Yasir M, Gzara L, Ahmad RZ. Assessment of antibacterial cellulose nanocomposites for water permeability and salt rejection. J Ind Eng Chem 2015;24:266–75. doi: 10.1016/j.jiec.2014.09.040.
[34] Lee H, Nishino M, Sohn D, Lee JS, Kim IS. Control of the morphology of cellulose acetate nanofibers via electrospinning. Cellulose 2018;25:2829–37. doi: 10.1007/s10570-018-1744-0.
[35] Perumal V, Hashim U, Gopinath SCB, Haarindraprasad R, Foo KL, Balakrishnan SR, Poopalan P. Spotted nanoflowers": gold-seeded zinc oxide nanohybrid for selective bio-capture. Sci Rep 2015;5:1–12. doi: 10.1038/srep12231.
[36] Haarindraprasad R, Hashim U, Gopinath SCB, Perumal V, Liu WW, Balakrishnan SR. Fabrication of interdigitated high-performance zinc oxide nanowire modified electrodes for glucose sensing. Anal Chim Acta 2016;925:70–81. doi: 10.1016/j.aca.2016.04.030.
[37] Zhang N, Ma W, Wu T, Wang H, Han D, Niu L. Edge-rich MoS_2 naonosheets rooting into polyaniline nanofibers as effective catalyst for electrochemical hydrogen evolution. Electrochim Acta 2015;180:155–63. doi: 10.1016/j.electacta.2015.08.108.
[38] Miao YE, Huang Y, Zhang L, Fan W, Lai F, Liu T. Electrospun porous carbon nanofiber@MoS_2 core/sheath fiber membranes as highly flexible and binder-free anodes for lithium-ion batteries. Nanoscale 2015;7:11093–101. doi: 10.1039/c5nr02711j.
[39] Veeramalai CP, Li F, Liu Y, Xu Z, Guo T, Kim TW. Enhanced field emission properties of molybdenum disulphide few layer nanosheets synthesized by hydrothermal method. Appl Surf Sci 2016;389:1017–22. doi: 10.1016/j.apsusc.2016.08.031.
[40] Wang F, Li G, Zheng J, Ma J, Yang C, Wang Q. Hydrothermal synthesis of flower-like molybdenum disulfide microspheres and their application in electrochemical supercapacitors. RSC Adv 2018;8:38945–54. doi: 10.1039/c8ra04350g.
[41] Hong CH, Ki SJ, Jeon JH, lian Che H, Park IK, Kee CD, Oh IK. Electroactive bio-composite actuators based on cellulose acetate nanofibers with specially chopped polyaniline nanoparticles through electrospinning. Compos Sci Technol 2013;87:135–41. doi: 10.1016/j.compscitech.2013.08.006.
[42] Yang L, Cui X, Zhang J, Wang K, Shen M, Zeng S, Dayeh SA, Feng L, Xiang B. Lattice strain effects on the optical properties of MoS2 nanosheets. Sci Rep 2014:4. doi: 10.1038/srep05649.
[43] Potla Durthi C, Rajulapati SB, Palliparambi AA, Kola AK, Sonawane SH. Studies on removal of arsenic using cellulose acetate–zinc oxide nanoparticle mixed matrix membrane. Int Nano Lett 2018;8:201–11. doi: 10.1007/s40089-018-0245-3.
[44] Chaudhary N, Khanuja M, Abid SSIslam. Hydrothermal synthesis of MoS_2 nanosheets for multiple wavelength optical sensing applications. Sens Actuat, A Phys 2018;277:190–8. doi: 10.1016/j.sna.2018.05.008.
[45] S.V.P. Vattikuti, P.C. Nagajyothi, K.C. Devarayapalli, K. Yoo, Applied surface science hybrid Ag / MoS2 nanosheets for efficient electrocatalytic oxygen reduction, 526 (2020) 1–9.
[46] Lv Q, Wang Y, Su C, Lakshmipriya T, Gopinath SCB, Pandian K, Perumal V, Liu Y. Human papilloma virus DNA-biomarker analysis for cervical cancer: signal enhancement by gold nanoparticle-coupled tetravalent streptavidin-biotin strategy. Int J Biol Macromol 2019;134:354–60. doi: 10.1016/j.ijbiomac.2019.05.044.
[47] Balasubramanian P, Balamurugan TST, Chen SM, Chen TW. Facile synthesis of orthorhombic strontium copper oxide microflowers for highly sensitive nonenzymatic detection of glucose in human blood. J Taiwan Inst Chem Eng 2017;81:182–9. doi: 10.1016/j.jtice.2017.10.040.
[48] Vasudevan M, Tai MJY, Perumal V, Gopinath SCB, Murthe SS, Ovinis M, Mohamed NM, Joshi N. Highly sensitive and selective acute myocardial infarction detection using aptamer-tethered MoS2 nanoflower and screen-printed electrodes. Biotechnol Appl Biochem 2020:1–10. doi: 10.1002/bab.2060.
[49] Subramani IG, Perumal V, Gopinath SCB, Mohamed NM, Joshi N, Ovinis M, Sze LL. 3D nanoporous hybrid nanoflower for enhanced non-faradaic redox-free electrochemical impedimetric biodetermination. J Taiwan Inst Chem Eng 2020. doi: 10.1016/j.jtice.2020.11.006.
[50] Balakrishnan SR, Hashim U, Letchumanan GR, Kashif M, Ruslinda AR, Liu WW, Veeradasan P, Haarindra Prasad R, Foo KL, Poopalan P. Development of highly sensitive polysilicon nanogap with APTES/GOx based lab-on-chip biosensor to determine low levels of salivary glucose. Sens Actuat, A Phys 2014;220:101–11. doi: 10.1016/j.sna.2014.09.027.
[51] Chen CJ, Liu JT, Chang SJ, Lee MW, Tsai JZ. Development of a portable impedance detection system for monitoring the growth of mouse L929 cells. J Taiwan Inst Chem Eng 2012;43:678–84. doi: 10.1016/j.jtice.2012.04.008.
[52] Wang X, Xing W, Feng X, Song L, Hu Y. MoS_2/polymer nanocomposites: preparation, properties, and applications. Polym Rev 2017;57:440–66. doi: 10.1080/15583724.2017.1309662.